Model Predictive Direct Power Control of Doubly Fed Induction Generator with Dead-Time Compensation

Van Quang Binh Ngo, Pedro Rodriguez-Ayerb, Sorin Olaru *
and Silviu-Iulian Niculescu **

** Laboratory of Signals and Systems,
CentraleSupélec-CNRS-UPS-Paris Saclay University, Gif-sur-Yvette
91192, France (e-mail: Binhvanquang.Ngo@supelec.fr,
Pedro.Rodriguez@centralesupelec.fr, Sorin.Olaru@centralesupelec.fr)
** Laboratory of Signals and Systems,
CNRS-CentraleSupélec-UPS-Paris Saclay University, Gif-sur-Yvette
91192, France (e-mail: Silviu.Niculescu@l2s.centralesupelec.fr.*

Abstract: The paper presents the control of a doubly fed induction generator connected with a three-level neutral point clamped inverter with compensation of dead-time effects. Model Predictive Direct Power Control is synthesized using a dynamical model of the doubly fed induction generator and three-level neutral point clamped inverter. The principle of the proposed control scheme is to use the dynamical model to compute predictions of the future values of the stator flux, rotor current and DC-link capacitor voltages for all possible configurations of voltage vectors. However, the dead-time to avoid the short circuit in the inverter also causes the modeling errors. Thus, by taking into account the dead-time in the model, it is possible compensate the dead-time effect of the switching devices. The active and reactive powers can be estimated based on the stator flux and the rotor current. The cost function considers the error between the active, reactive powers and their references, balance the DC-link capacitor voltage and reduce the switching frequency and common-mode voltage. The optimal switching state that minimizes the cost function is selected and applied to the inverter. The simulation results were carried out with Matlab under different conditions of wind speed and verifying the effectiveness of the proposed method.

Keywords: Power Plants and Power Systems, Control of renewable energy resources, Application of power electronics, Intelligent control of power systems and Optimal operation and control of power systems.

1. INTRODUCTION

Nowadays, to the best of the author's knowledge, the global wind energy capacity has increased rapidly and became one of the fastest developing renewable technologies. Most of the major wind turbine manufactures are developing larger wind turbines in the 1.5-6 MW range. For such an application, doubly fed induction generator (DFIG) represents an attractive solution due to its advantages: for instance, it allows the power converter to deal with approximately 30% of the generator power, reduces converter cost and power lost (Fig. 1) (Abad et al. (2011)). By using this configuration, it is possible to allow both bidirectional active and reactive power flow from the rotor side to grid through the rotor side converter (RSC) and grid side converter (GSC). Furthermore, from the technological point of view, the three-level neutral point-clamped (3L-NPC) inverter structure represents a good solution for high power due to its advantages: reduction of the total harmonic distortion (THD) and increasing the capacity of the inverter due to a decreased voltage applied to each component.
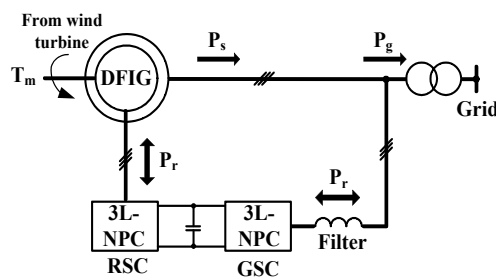
Fig. 1. Schematic diagram of DFIG based wind generation systems (Abad et al. (2011))

Several approaches have been proposed to control DFIG for wind energy generation. Most of the existing control methods use the classical vector control based on the orientation of the flux stator (stator flux oriented) or stator voltage (stator voltage oriented). This method allows controlling independently the electromagnetic torque or active power and reactive power by means the components of the rotor current (Abad et al. (2011)). However, one drawback of this method is that its performance depends on accurate machine parameters such as stator and rotor

resistance and mutual inductance. Next, another drawback of using PI controller is the necessity of tuning of the gains in the whole operating range of wind speed. In addition, a complex modulation technique along with the DC-link capacitor voltages balancing is required to apply these techniques to 3L-NPC inverter.

Recently, direct torque control (DTC) or direct power control (DPC) (Xu and Cartwright (2006)) have been proposed to improve the controller performance. These methods used the hysteresis control and the inverter switching states, selected from a look-up table (LUT) based on the errors between the reference and estimated values, and rotor or stator flux position. Therefore, these methods do not require the current control loops and space vector modulation. Nevertheless, the drawback of LUT is that it has large active and reactive power ripple and switching frequency variation. In addition, a high-sampling frequency is used for DTC/DPC to guarantee acceptable steady-state and dynamic performances. To overcome this problem several techniques have been developed such as using DPC with space vector modulation (SVM) (Kazemi et al. (2010)), predictive control strategy (Sayritupac et al. (2015)) and model predictive power control (?). Moreover, the dead-time effect will distort the output voltage, neutral-point voltage and current. Thus, a dead-time compensation is necessary to be added into the control scheme (Irnura et al. (2012); Zhou and Rouaud (1999)). In this context, model predictive control is an alternative control technique that has been recently applied to DFIG due to its advantages, such as easy inclusion of non-linearities in the model, delay and dead-time compensation and no need of current control loops (Errouissi et al. (2016); Sun and Wang (2016)).

The present paper proposes the model predictive direct power control (MPDPC) to control the active and reactive power for DFIG connected to a 3L-NPC inverter while maintaining the balance between the DC link capacitor voltage, reducing the switching frequency and the common-mode voltage. These objectives are accomplished through the cost function in a predictive control strategy. In this paper, we focus on the modelling of errors caused by dead-time induced by the physical switching mechanism. With this approach, the model to predict the inverter ouput voltage and neutral-point voltage takes into account the dead-time take of the conveter to compensate its effects. No current loops are considered and the inverter switches are directly obtained from the cost function minimization. This control allows improving the quality of the power regulation and minimizing the switching losses. In order to reduce the computational effort, a control horizon of two is used for the prediction, where only combination of inputs having a difference of one switch in the inverter is considered.

The remaining paper is organized as follow: Section 2 presents the mathematical model of direct power control with dead-time compensation for a DFIG connected to a 3L-NPC. Next, section 3 details the proposed control method. In section 4, simulation results are represented and analyzed and, finally, section 5 draws the conclusion.

2. MODEL OF DFIG CONNECTED 3L-NPC INVERTER

The doubly fed induction generator (DFIG) can be modelled by the equivalent circuit in dq coordinate (see Abad et al. (2011)) based on stator fluxed orientation. The stator and rotor voltage vectors can be described from Fig. 2 as follows:

$$u_s^{dq} = R_s i_s^{dq} + \frac{d\psi_s^{dq}}{dt} + j\omega_s \psi_s^{dq} \qquad (1)$$

$$u_r^{dq} = R_r i_r^{dq} + \frac{d\psi_r^{dq}}{dt} + j\omega_r \psi_r^{dq}. \qquad (2)$$

where u_s^{dq}, i_s^{dq}, ψ_s^{dq} are the stator voltage, current and flux vector in dq reference frame while u_r^{dq}, i_r^{dq}, ψ_r^{dq} are the rotor counterparts with respect to the stator. R_s, R_r are the stator resistance and the rotor resistance referred to the stator, ω_s, ω_m are the synchronous speed of stator flux and angular rotor speed (rad/s), $\omega_r = \omega_s - \omega_m = s\omega_s$ is the rotor angular frequency, with the coefficient s denoting the slip.
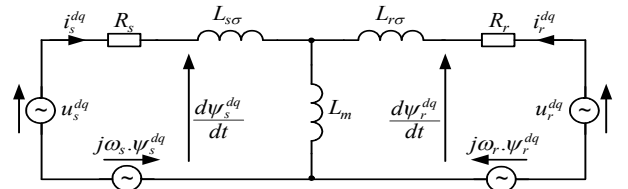

Fig. 2. Equivalent circuit of the DFIG in dq reference frame

The relationship between fluxes and currents is:

$$\psi_s^{dq} = L_s i_s^{dq} + L_m i_r^{dq}, \qquad (3)$$

$$\psi_r^{dq} = L_r i_r^{dq} + L_m i_s^{dq}, \qquad (4)$$

with L_s and L_r are the stator and rotor inductances and L_m the magnetizing inductance.

By substituting the stator current i_s^{dq} from equation (3) into equation (1), the stator flux dynamics can be expressed as follows:

$$\frac{d\psi_s^{dq}}{dt} = \frac{1}{T_s} \left(-\left(1 + j\omega_s T_s\right)\psi_s^{dq} + L_m i_r^{dq} + T_s u_s^{dq} \right), \quad (5)$$

where $T_s = \frac{L_s}{R_s}$ is the time constant of the stator.

By substituting equation (5) and the rotor flux ψ_r^{dq} from equations (3) and (4) into equation (2), the dynamics of the rotor currents are represented as follows:

$$\frac{di_r^{dq}}{dt} = \frac{1}{\sigma L_r} \left(\psi_s^{dq} \left(\frac{L_m}{L_s T_s} + j\omega_m \frac{L_m}{L_s} \right) + u_r^{dq} \right) \qquad (6)$$
$$ - \frac{1}{\sigma L_r} \left(i_r^{dq} \left(R_\sigma + j\omega_r \sigma L_r \right) + \frac{L_m}{L_s} u_s^{dq} \right),$$

where $R_\sigma = R_r + L_m^2/L_s T_s$, $\sigma = 1 - L_m^2/L_s L_r$ is the leakage coefficient.

Based on equations (5) and (6), the dynamical model of DFIG can be expressed in matrix form as below:

$$\dot{x} = A(\omega_s, \omega_m)x + Bu, \qquad (7)$$

where $x = \begin{bmatrix} \psi_{ds} \\ \psi_{qs} \\ i_{dr} \\ i_{qr} \end{bmatrix}$, $u = \begin{bmatrix} u_{ds} \\ u_{qs} \\ u_{dr} \\ u_{qr} \end{bmatrix}$,
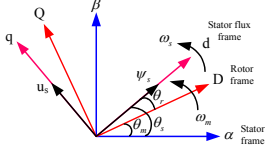
Fig. 3. Vector representation in different reference frame

$$A(\omega_s, \omega_m) = \begin{bmatrix} -\dfrac{1}{T_s} & \omega_s & \dfrac{L_m}{T_s} & 0 \\ -\omega_s & -\dfrac{1}{T_s} & 0 & \dfrac{L_m}{T_s} \\ \dfrac{L_m}{L_s T_s \sigma L_r} & -\dfrac{\omega_m L_m}{L_s \sigma L_r} & -\dfrac{R_\sigma}{\sigma L_r} & \omega_r \\ \dfrac{\omega_m L_m}{\sigma L_s L_r} & \dfrac{L_m}{L_s T_s \sigma L_r} & -\omega_r & -\dfrac{R_\sigma}{\sigma L_r} \end{bmatrix}, \quad (8)$$

$$B = \begin{bmatrix} 1 & 0 & 0 & 0 \\ 0 & 1 & 0 & 0 \\ -\dfrac{L_m}{\sigma L_s L_r} & 0 & \dfrac{1}{\sigma L_r} & 0 \\ 0 & -\dfrac{L_m}{\sigma L_s L_r} & 0 & \dfrac{1}{\sigma L_r} \end{bmatrix}.$$

Since the stator is connected to the grid, the stator flux is a function of the grid voltage in steady state. Neglecting the small drop in the stator resistance due to its relatively small value in comparison with the the stator reactance ($R_s << \omega_s L_s$), we can obtain:

$$u_s^{dq} \approx \frac{d\psi_s^{dq}}{dt} \approx \frac{d\left(\left|\psi_s^{dq}\right| e^{j\omega_s}\right)}{dt} \approx j\omega_s \psi_s^{dq}. \quad (9)$$

The system being oriented with stator flux (Fig. 3), and taking into account the equation (9), the component of stator flux can be derived as follows (Abad et al. (2011)):

$$u_{ds} = \psi_{qs} = 0; \ u_{qs} = \hat{U}_g \approx \omega_s \psi_s^{dq} \approx \omega_s \psi_{ds}, \quad (10)$$

where $\hat{U}_g$ is the magnitude of the grid voltage.

The active and reactive powers in the stator can be expressed as below:

$$P_s = \frac{3}{2}\left(u_{ds}i_{ds} + u_{qs}i_{qs}\right) = -\frac{3}{2}\psi_{ds}\frac{L_m}{L_s}\omega_s i_{qr}$$
$$Q_s = \frac{3}{2}\left(u_{qs}i_{ds} - u_{ds}i_{qs}\right) = \frac{3}{2}\hat{U}_g\left(\frac{\psi_{ds}}{L_s} - \frac{L_m}{L_s}i_{dr}\right). \quad (11)$$

Furthermore, by neglecting the coper power losses in the stator and rotor resistance, the active and reactive powers in stator and rotor can be derived (see Abad et al. (2011)) as follows:

$$P_r = -sP_s; \ Q_r = sQ_s. \quad (12)$$

In addition, the rotor voltage which will be injected into DFIG, is also the output voltage of 3L-NPC inverter shown in Fig. 4. The inverter output voltage in rotor reference frame u_{inv}^{DQ} is defined as:

$$u_{inv}^{DQ} = \frac{2}{3}\left(u_{AZ} + au_{BZ} + a^2 u_{CZ}\right), \quad (13)$$

with $a = e^{j2\pi/3} = -\frac{1}{2} + j\frac{\sqrt{3}}{2}$.

The inverter output voltage u_{AZ}, u_{BZ} and u_{CZ} of 3L-NPC inverter are calculated (see Ngo et al. (2016)) as a function of the DC link voltage U_{dc} and switching states S_x:

$$u_{AZ} = S_a \frac{U_{dc}}{2}; u_{BZ} = S_b \frac{U_{dc}}{2}; u_{CZ} = S_c \frac{U_{dc}}{2}, \quad (14)$$
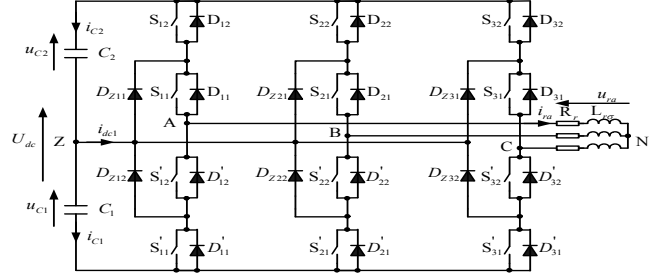

Fig. 4. The configuration of the rotor of DFIG connected 3L-NPC inverter

where S_x represents the state of a leg and has three possible values: [-1, 0, 1] or [N, O, P].

Consequently, the rotor voltage referred to the stator in "dq" reference frame (u_r^{dq}) can be calculated by using rotational transformation as (Abad et al. (2011)):

$$u_r^{dq} = K u_{inv}^{DQ} e^{-j\theta_r}, \quad (15)$$

where K is the ratio of the stator voltage to the rotor voltage of the DFIG.

The rotor current referred to the stator in "dq" reference frame (i_r^{dq}) can be calculated from the rotor current in rotor reference (i_r^{DQ}) by using rotational transformation:

$$i_r^{dq} = \frac{1}{K} i_r^{DQ} e^{-j\theta_r}. \quad (16)$$

In the real implementation of the 3L-NPC inverter, considering a dead-time in the modeling is necessary to prevent the simultaneous conduction of two switching devices in each leg of the inverter. The dead-time causes output current waveform distortion and increases the THD, especially with high switching frequency (Kuznietsov et al. (2015); Irnura et al. (2012)). The voltage vector during the dead-time is determined according to the state between previous switching state and present switching state and the sign of the phase current. For example, in switching state [O], switches S_{11} and S'_{12} are turned "on". The clamping diode D_{Z11} is turned "on" by the positve load current ($i_{ra} > 0$). For ideal case without dead-time, the switch S'_{12} is turned "off" and S_{12} is turned "on" simultaneously, so that the output voltage changes from zero to $U_{dc}/2$ at the same time. If the dead-time is considered, the real gate signals and output voltage approximation are shown in Fig. 5(a). During the dead-time interval, S'_{12} is being turned "off" and the path of i_{ra} remains unchanged. Thus, the output actual voltage is clamped is zero. After S_{12} is turned "on" (switching state [P]), the load current is commutated from D_{Z11} to S_{12} and the output voltage switches to $U_{dc}/2$ (Fig. 6(a)). Hence, the real output voltage is reduced with the mean value U_{dt} and shown with the rectangular pattern in Fig. 5(a). In brief, the influence of dead-time on output voltage can be illustrated in Fig. 5. Thus, in order to compensate the dead-time, the real voltage applied during a sampling period T_{sp} can be represented by a voltage U_{dt} during the dead-time t_d and the predicted voltage vector with the rest time T_{sp} - t_d (Irnura et al. (2012)). The real output voltage of one phase $u_{xz-real}$ can be expressed as follows:

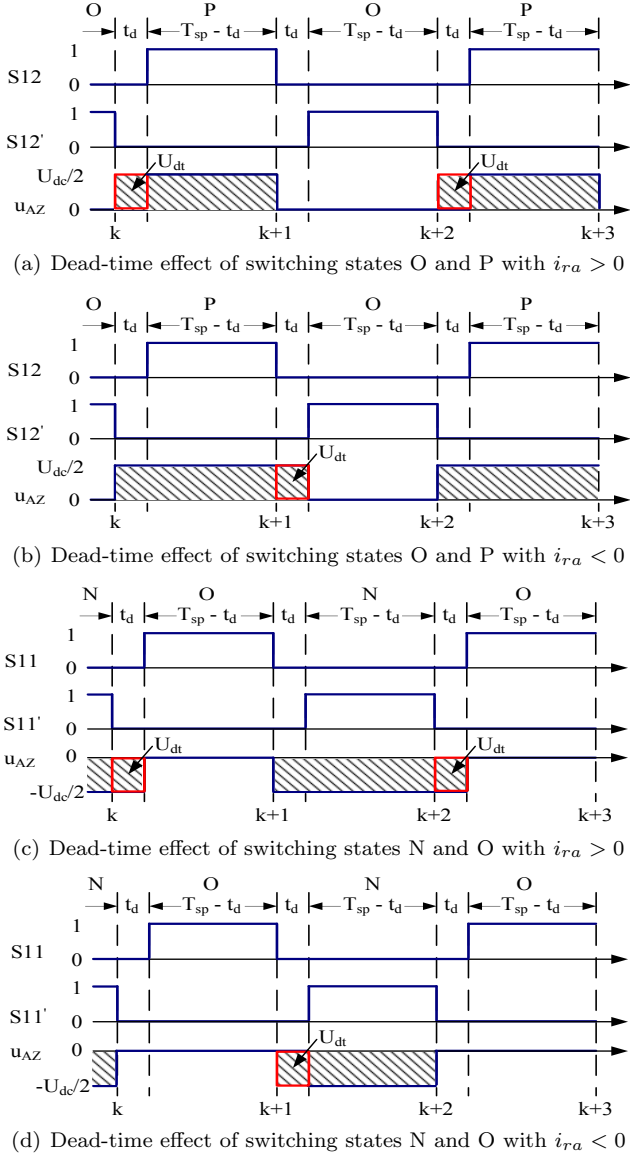(i) $(S_x(k-1) = 0) \& (S_x(k) = 1)$,
(ii) $(S_x(k-1) = -1) \& (S_x(k) = 0)$,

(a) Dead-time effect of switching states O and P with $i_{ra} > 0$

(b) Dead-time effect of switching states O and P with $i_{ra} < 0$

(c) Dead-time effect of switching states N and O with $i_{ra} > 0$

(d) Dead-time effect of switching states N and O with $i_{ra} < 0$

Fig. 5. The effect of dead-time on inverter output voltage

(a) Commutation from swiching state O to P with $i_{ra} > 0$

(b) Commutation from swiching state O to P with $i_{ra} < 0$

(c) Commutation from swiching state N to O with $i_{ra} > 0$

(d) Commutation from swiching state N to O with $i_{ra} < 0$

Fig. 6. Commutation during the dead-time

(iii) $(S_x(k-1) = 1) \,\&\, (S_x(k) = 0)$,
(iv) $(S_x(k-1) = 0) \,\&\, (S_x(k) = -1)$,

$$u_{xz\_real}(k) = \begin{cases} -U_{dt} + u_{xz}(k) \\ \quad \text{if satisfy } (\text{sign}(i_{rx}) > 0) \,\&\, ((i) \vee (ii)), \\ U_{dt} + u_{xz}(k) \\ \quad \text{if satisfy } (\text{sign}(i_{rx}) < 0) \,\&\, ((iii) \vee (iv)), \\ u_{xz}(k) \quad \text{otherwise}, \end{cases}$$
(17)

where u_{xz}, i_{rx} are the inverter output voltage and rotor current of one phase $x = a, b, c$; $U_{dt} = \dfrac{t_d}{T_{sp}} \dfrac{U_{dc}}{2}$.

Based on the configuration in Fig. 4, the dynamic of neutral-point voltage (Z) is obtained based on the rotor currents and the switching states of 3L-NPC inverter (Ngo et al. (2016)):

$$\frac{du_z}{dt} = -\frac{1}{2C} i_{dc1}$$
(18)

$$= -\frac{1}{2C} \Big((1 - |S_a|) i_{ra} + (1 - |S_b|) i_{rb} + (1 - |S_c|) i_{rc} \Big)$$

Furthermore, the dead-time can also affect the neutral-point voltage because of the different neutral-point current as shown in Fig. 6 (Sprenger et al. (2013)). Summarizing, the neutral-point curent during the dead-time only exists when there are transitions between switching states [O] and [P] with positive load current or between switching states [N] and [O] with negative load current or remain the switching state [O]. Thus, the neutral-point current of one phase during the dead-time can be described:

(v) $(\text{sign}(i_{rx}) > 0) \,\&\, ((i) \vee (ii))$,
(vi) $(\text{sign}(i_{rx}) < 0) \,\&\, ((iii) \vee (iv))$,
(vii) $(S_x(k-1) = 0) \,\&\, (S_x(k) = 0)$,

$$i_{dc1x\_dt} = \begin{cases} \dfrac{t_d}{T_{sp}} i_{rx}, & \text{if satisfy } ((v) \vee (vi) \vee (vii)), \\ 0, & \text{otherwise}, \end{cases}$$
(19)

where i_{dc1x_dt} is the neutral-point current during the dead-time of one phase $x = a, b, c$.

Similarly, the real neutral-point current during a sampling period is expressed by the neutral-point current during the dead-time t_d and the predicted current with the rest time $T_{sp} - t_d$:

$$i_{dc1\_real} = i_{dc1a\_dt} + i_{dc1b\_dt} + i_{dc1c\_dt} + \frac{T_{sp} - t_d}{T_{sp}} i_{dc1}. \quad (20)$$

By using the equation (18), the neutral-point voltage for compensate the dead-time can be rewritten:

$$\frac{du_{z\_real}}{dt} = -\frac{1}{2C} i_{dc1\_real}. \quad (21)$$

In an inverter driven system, the common-mode voltage (u_{cm}) is defined as the voltage between the rotor neutral (N) and the neutral-point voltage (Z). Thus, the common-mode voltage (CMV) can be expressed as follows (Rodriguez and Cortes (2012)):

$$u_{cm} = \frac{u_{AZ} + u_{BZ} + u_{CZ}}{3}. \quad (22)$$

Therefore, a compensation for the dead-time can be established for MPDPC. By using modified voltage vector in equation (17), (21) and (22), we can predict the power taking into account the dead-time voltage at switching state.

3. MODEL PREDICTIVE DIRECT POWER CONTROL APPLIED TO DFIG CONNECTED 3L-NPC

The aim of the predictive direct power control scheme is to minimize the error between the predicted active and reactive powers and their reference values, to maintain voltage balance of the capacitor and to reduce the switching frequency and common-mode voltage. In order to achieve these objectives, the cost function for the DFIG connected 3L-NPC inverter with two-step prediction can be expressed as follows (Rodriguez and Cortes (2012)):

$$g = |P_s^*(k+2) - P_s^p(k+2)| + |Q_s^*(k+2) - Q_s^p(k+2)|$$
$$+ \lambda_{dc} |u_z^p(k+2)| + \lambda_{cm} |u_{cm}| + \lambda_n n_c \quad (23)$$

where λ_{dc}, λ_n and λ_{cm} are the weighting factors of the capacitor voltage balancing, the reduction of commutation and CMV. n_c penalizes the number of switching changes when the switching state $S(k)$ is applied compared with previous state $S(k-1)$. It can be expressed as:

$$n_c = |S_a(k) - S_a(k-1)| + |S_b(k) - S_b(k-1)|$$
$$+ |S_c(k) - S_c(k-1)|. \quad (24)$$

In the real-time implementation of the control scheme, the calculation time of the control law will induce some sample time delay in the actuation (Sun and Wang (2016); Errouissi et al. (2016)). Several studies to address the delay compensation, but this particular aspect is not the focus of this paper. A simple solution to compensate the computational delay is to compute at time instant k the cost function corresponding to time instant $k+1$ using an estimation of the state at time $k+1$ and then the optimal switching state is applied at time $k+1$. In this paper, we used the method proposed by Ngo et al. (2016) to reduce the computational effort and allow a straightforward implementation.

The equation (7) can be discretized considering T_{sp} as a sampling period and k as the sampling time by using zero-order hold (ZOH) with no delay:

$$x(k+1) = A_d x(k) + B_d u(k) \quad (25)$$

where

$$A_d = e^{AT_{sp}}, B_d = \int_0^{T_{sp}} e^{A(T_{sp} - d\tau)} B d\tau \simeq B T_{sp}. \quad (26)$$

Since the active and reactive powers references are DC quantities, to reduce the computational time and the oscillations in the reference powers when a sudden change occurs, the extrapolation can be simplified as follows:

$$P_s^*(k+2) = P_s^*(k); Q_s^*(k+2) = Q_s^*(k). \quad (27)$$

Finally, the objective of proposed predictive control can be obtained by evaluating some appropriate cost function for all considered input combinations (see algorithm 1).

Algorithm 1 Algorithm of model predictive direct power control for DFIG connected 3L-NPC inverter

Measure $i_s(k)$, $i_r(k)$, $u_z(k)$, $u_s(k)$, ω_m and U_{dc}; Read the reference values $P_s^*(k)$ and $Q_s^*(k)$
Estimation of stator flux $\psi_{ds}(k)$; Extrapolation of references $P_s^*(k+2)$, $Q_s^*(k+2)$ and $u_s^{dq}(k+1)$
%comment: x_{opt}, g_{opt} are the optimal values of the switching states and cost function%
Initialize optimal values: x_{opt}, g_{opt}
Predict stator flux: $\psi_{ds}^p(k+1)$
for $i = 1$ to 27 **do**
    Compute predictions with dead-time compensation: $i_{dr}^p(k+1)$, $i_{qr}^p(k+1)$ and $u_z^p(k+1)$
    Estimate the values: n_c and u_{cm}
    Predict corresponding switching transitions
%comment: m = length(corresponding switching transitions)
    for $j = 1$ to m **do**
        Predict: $i_{dr}^p(k+2)$, $i_{qr}^p(k+2)$, $\psi_{ds}^p(k+2)$ and $u_z^p(k+2)$
        Estimation of power: $P_s^p(k+2)$ and $Q_s^p(k+2)$
        Compute the cost function g
        if $g < g_{opt}$ **then**
            $g_{opt} = g; x_{opt} = i$
        end if
    end for
end for
Store the present value of x_{opt} and apply S_a, S_b, S_c considering the dead-time

---

4. SIMULATION RESULTS

In order to validate the effectiveness of the model predictive direct power control (MPDPC) strategy with dead-time compensation for DFIG under different modes of speed operation, the whole control scheme has been simulated using MATLAB/Simulink and the SimPowerSystems toolbox with the parameters as indicated in Table A.1.

With the aim to evaluate the steady state performance, the mean absolute percentage error (MAPE) is used. This quantity can be expressed as follows:

$$MAPE = \frac{1}{n} \sum_{i=1}^{n} \left| \frac{y_i^* - y_i}{y_i^*} \right|, \quad (28)$$

where y_i^* is the reference vector and y_i is the measurement vector.

On the other hand, the average switching frequency per semiconductor ($\overline{f_{sw}}$) = 1 kHz is calculated according to the
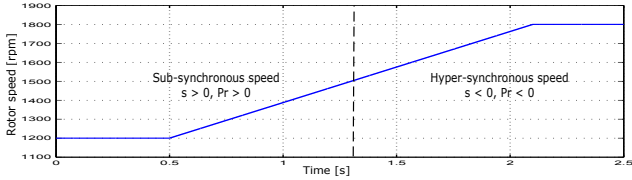
Fig. 7. Rotor angular speed time response

following expression proposed in (Rodriguez and Cortes (2012)):

$$\overline{f_{sw}} = \sum_{x=a,b,c} \frac{f_{sw_{1x}} + f_{sw_{2x}}}{6}, \qquad (29)$$

where $f_{sw_{1x}}$, $f_{sw_{2x}}$ are the switching frequencies of each upper switch.

With the purpose of control the power factor (PF), the reactive power reference is given by:

$$Q_{s\_ref} = P_{s\_ref} \frac{\sqrt{1 - PF^2}}{PF}. \qquad (30)$$

In our comparison, the DFIG was assumed to be in speed control, i.e., the rotor speed is set externally, and has slow changes because of the large inertia of the wind turbine. In order to observe the dynamics response of the DFIG, various active and reactive power steps with rotor speed varying from 1200 to 1800 rpm (Fig. 7) were carried out. The active power reference is changed from -2 MW to -1 MW at 1.5 s and from -1 MW to -1.5 MW at 2 s (Fig. 8(a)). While the reactive power reference is changed from -1.24 MVar to 0.62 MVar at 1.5 s and from 0.62 MVar to 0 Var at 2 s, corresponding with the change of power factor from 1 to a leading (0.85) or lagging (-0.85). When the rotor speed of the generator is greater than synchronous speed, the slip is negative (s = -0.2), thus, the rotor power P_r will be transferred from the generator rotor to the grid through the rotor converters of the DFIG, whereas the RSC operates as a rectifier and the GSC as an inverter. The powers delivered to the grid P_g and Q_g which are the sum of the stator and rotor powers are illustrated in Figs. 8(a) and 8(b). On the contrary, the slip is positive (s = 0.2) with sub-synchronous speed. This positive slip means that the rotor power P_r will be positive and will be received from the grid through the converters in which the RSC operates as an inverter and the GSC as a rectifier (Fig. 8). In addition, Figs. 8(a) and 8(b) indicate that the active power is tracking their references with fast dynamics and without affecting the reactive power. The mean absolute percentage error of active and reactive power for uncompensated case are 1.68% and 2.25%, whereas, for the proposed method they are 1.65%, and 2.22%, respectively.

For further verification of the dead-time compensation method, the spectrum of the stator current is analyzed and compared for the uncompensated and compensated case in Fig. 9. For the uncompensated case in Fig. 9(a), the amplitude of the order harmonic is larger, which is caused by the dead-time effect. The THD for the uncompensated stator current is around 4.3%. But for the compensated current in Fig. 9(b), the order harmonic components have been largely reduced, especially the 21th, 22th and 23th order harmonic. Also the THD for the stator current is
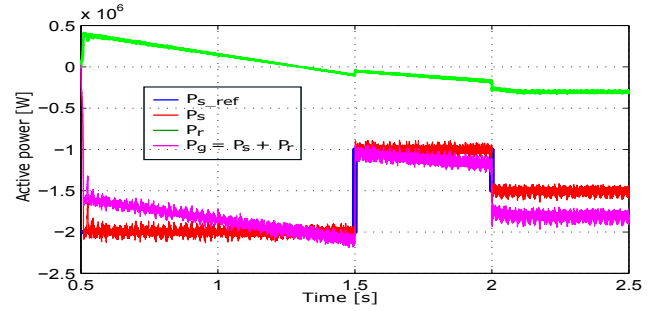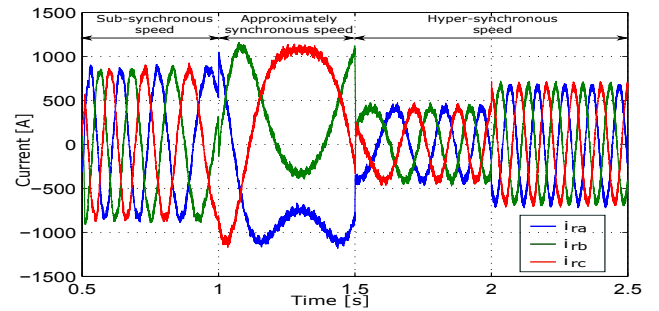

(a) Generated active power
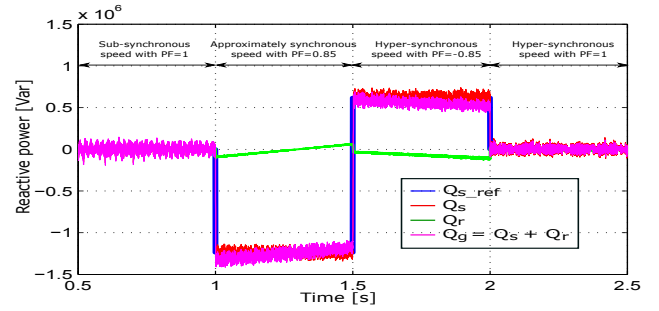
(b) Generated reactive power
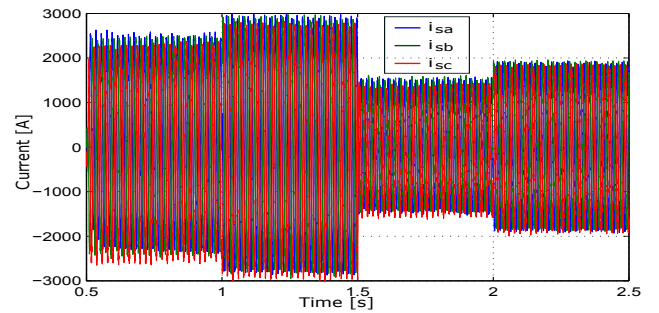
(c) Stator current

(d) Rotor current

Fig. 8. The dynamic response of the power and current with rotor speed variation

reduced from 4.3 % to 3.03 % which is under the 5% limit required by the IEEE 519 standards.

5. CONCLUSIONS

In this paper, a new direct power control with dead-time compensation method for DFIG system has been proposed to control the active and reactive powers directly. First, the mathematical model including the dead-time errors is established, and then the cost function, which contains the power errors, the capacitor voltage balancing and the reduction of the switching frequency, is proposed. In order to verify the performance of control scheme, there is a

(a) Without compensation
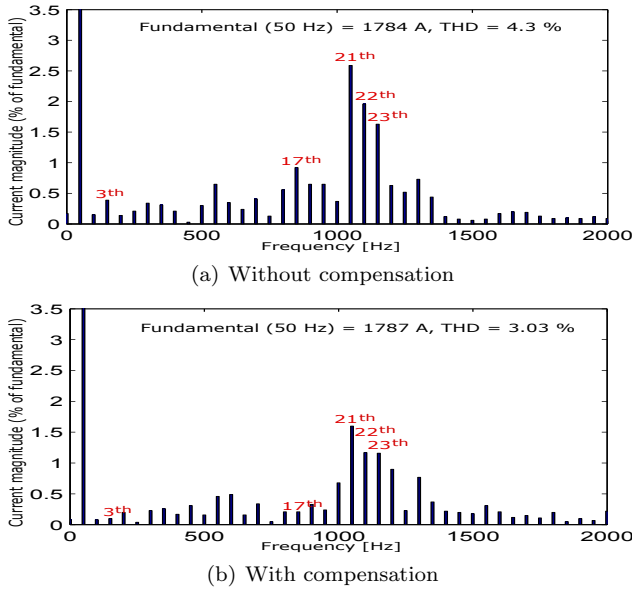

(b) With compensation

Fig. 9. Stator current spectrum with and without compensation

comparison between the case without compensation and the proposed method. The simulation results show that this method can successfully track the active and reactive powers, maintain their balanced capacitor voltages, reduce the switching frequency and common-mode voltage. Furthermore, by using the proposed method we can reduce the voltage error due to switching dead-time while maintaining an acceptable quality of current and power. The linear PI controllers for the power, current loops and the modulation block are further eliminated. In addition, by maintaining the device switching frequency below 1 kHz, the proposed method is an interesting alternative to control the DFIG connected 3L-NPC inverter for megawatt range wind power applications.

REFERENCES

Abad, G., Lopez, J., Rodriguez, M.A., Marroyo, L., and Iwanski, G. (2011). *Doubly fed induction machine-Modelling and control for wind energy generation.* John Wiley and Sons.

Errouissi, R., Al-Durra, A., Muyeen, S.M., Leng, S., and Blaabjerg, F. (2016). Offset-free direct power control of DFIG under continuous-time model predictive control. *IEEE Transaction On Power Electronics*.

Filho, A.J.S. and Ruppert, E. (2010). A deadbeat active and reactive power control for doubly fed induction generator. *Electric Power Components and Systems*, 38(5), 592–602.

Hu, J. and Yuan, X. (2012). Vsc-based direct torque and reactive power control of doubly fed induction generator. *Journal Renewable Energy*, 40, 13–23.

Irnura, A., Takahashi, T., Fujitsuna, M., Zanma, T., and Doki, S. (2012). Dead-time compensation in model predictive instantaneous-current control. In *Proceeding of 38th Annual Conference of IEEE Industrial Electronics Society (IECON 2012)*, 5037–5042.

Kazemi, M.V., Yazdankhah, A.S., and Kojabadi, H.M. (2010). Direct power control of DFIG based on discrete space vector modulation. *Journal Renewable Energy*, 35, 1033–1042.

Kuznietsov, A., Wolf, S., and Happek, T. (2015). Model predictive control of a voltage source inverter with compensation of deadtime effects. In *Proceeding of 2015 IEEE International Conference on Industrial Technology (ICIT)*, 2532–2536.

Ngo, B.Q.V., Rodriguez-Ayerbe, P., and Olaru, S. (2016). Model predictive direct power control for doubly fed induction generator based wind turbines with three-level neutral-point clamped inverter. In *42nd Annual Conference on IEEE Industrial Electronics Society IECON*.

Rodriguez, J. and Cortes, P. (2012). *Predictive Control of Power Converters and Electrical Drives.* John Wiley.

Sayritupac, J., Albanez, E., Rengifo, J., Aller, J.M., and Restrepo, J. (2015). Predictive control strategy for DFIG wind turbines with maximum power point tracking using multilevel converters. In *Proceeding of workshop on Power Electronics and Power Quality Applications (PEPQA)*, 1–6. Bogota.

Sprenger, M., Barth, T., Alvarez, R., Tannhaeuser, M., and Bernet, S. (2013). Experimental verification of direct dead-time control and DC-link neutral-point balancing of a three level neutral-point-clamped (3l-npc) vsc. In *Proc. IEEE Energy Conversion Congress and Exposition*, 409–413.

Sun, D. and Wang, X. (2016). Low-complexity model predictive direct power control for DFIG under both balanced and unbalanced grid conditions. *IEEE Transactions on Industrial Electronics*, 63(8), 5186–5196.

Xu, L. and Cartwright, P. (2006). Direct active and reactive power control of DFIG for wind energy generation. *IEEE Transactions on Energy Conversion*, 21(3), 750–758.

Zhou, D. and Rouaud, D.G. (1999). Dead-time effect and compensations of three-level neutral point clamp inverters for high-performance drive applications. *IEEE Transactions on Power Electronics*, 14(4), 782–788.

Appendix A. PARAMETERS FOR DFIG, CONTROLLER AND SWITCHING DEVICES

Table A.1. Simulation parameters

Parameter	Value	Description
P_{rated}	2 [MW]	Rated stator three phase active power
$U_{s-rated}$	690 [V]	Line to line nominal stator voltage
$U_{r-rated}$	2070 [V]	Line to line nominal rotor voltage
$I_{s-rated}$	1760 [A]	Each phase nominal stator current
$n_{s-rated}$	1500 [rpm]	Synchronous speed
p	2	The number pairs of poles
R_s	2.6 [mΩ]	Stator resistance
R_r	2.9 [mΩ]	Rotor resistance
$L_{\sigma s}$	87 [μH]	Stator leakage inductance
$L_{\sigma r}$	87 [μH]	Rotor leakage inductance
L_m	2.5 [mH]	Mutual inductance
J	0.314 [kg.m^2]	Moment of inertia
f_s	50 [Hz]	Frequency of the grid
f_{sp}	10 [kHz]	Sampling frequency of MPDPC
U_{dc}	1200 [V]	DC link voltage
C	16000 [μ F]	DC link capacitor
t_d	5 [μs]	Dead-time of IGBT
V_f, V_{fd}	0.8; 0.1 [V]	Forward voltage of IGBT and diode
λ_{dc}	200	Weighting factor of the voltage balancing
λ_n	35000	Switching frequency reduction factor
λ_{cm}	200	Weighting factor of the reduction of CMV